University of Glasgow

Mortimer, E., Kirstein, L. A., Stuart, F. M. and Strecker, M. R. (2016) Spatio-temporal trends in normal-fault segmentation recorded by low-temperature thermochronology: Livingstone fault scarp, Malawi Rift, East African Rift System. *Earth and Planetary Science Letters*, 455, pp. 62-72. (doi:10.1016/j.epsl.2016.08.040)

This is the author's final accepted version.

There may be differences between this version and the published version. You are advised to consult the publisher's version if you wish to cite from it.

http://eprints.gla.ac.uk/128684/

Deposited on: 20 September 2016

Enlighten – Research publications by members of the University of Glasgow
http://eprints.gla.ac.uk

*Manuscript
Click here to view linked References

Spatio-temporal trends in normal-fault segmentation recorded by low-temperature thermochronology: Livingstone fault scarp, Malawi Rift, East African Rift System.

*Estelle Mortimer[1,2], Linda A. Kirstein[3], Finlay M. Stuart[4], and Manfred R. Strecker[1].

[1] Institut für Erd- und Umweltwissenschaften Universität Potsdam, Potsdam, Germany

[2] Present address: School of Earth and Environment, University of Leeds, Woodhouse Lane, Leeds, UK

[3] School of Geosciences, University of Edinburgh, West Mains Road, Edinburgh, EH9 3FE, UK

[4]Isotope Geosciences Unit, Scottish Universities Environmental Research Centre, East Kilbride, Scotland, UK

*Corresponding author; e.j.mortimer@leeds.ac.uk

Abstract

The evolution of through-going normal-fault arrays from initial nucleation to growth and subsequent interaction and mechanical linkage is well documented in many extensional provinces. Over time, these processes lead to predictable spatial and temporal variations in the amount and rate of displacement accumulated along strike of individual fault segments, which should be manifested in the patterns of footwall exhumation.

Here, we investigate the along-strike and vertical distribution of low-temperature apatite (U-Th)/He (AHe) cooling ages along the bounding fault system, the Livingstone fault, of the Karonga Basin of the northern Malawi Rift. The fault evolution and linkage from rift initiation to the present day has been previously constrained through investigations of the hanging wall basin fill. The new cooling

ages from the footwall of the Livingstone fault can be related to the adjacent depocenter evolution and across a relay zone between two palaeo-fault segments. Our data are complimented by published apatite fission-track (AFT) data and reveal significant variation in rock cooling history along-strike: the center of the footwall yields younger cooling ages than the former tips of earlier fault segments that are now linked. This suggests that low-temperature thermochronology can detect fault interactions along strike. That these former segment boundaries are preserved within exhumed footwall rocks is a function of the relatively recent linkage of the system.

Our study highlights that changes in AHe (and potentially AFT) ages associated with the along-strike displacement profile can occur over relatively short horizontal distances (of a few kilometers). This is fundamentally important in the assessment of the vertical cooling history of footwalls in extensional systems: temporal differences in the rate of tectonically driven exhumation at a given location along fault strike may be of greater importance in controlling changes in rates of vertical exhumation than commonly invoked climatic fluctuations.

Keywords: Apatite Helium thermochronology; normal-fault evolution; fault linkage; East African Rift System

1. Introduction

The displacement across a crustal-scale normal-fault is accommodated by a combination of hanging wall subsidence and, as a consequence of isostatic adjustments, to a lesser extent corresponding footwall uplift (e.g., Jackson and McKenzie, 1983; Walsh and Watterson, 1987; Stein and Barrientos, 1985). This

process leads to the vertical exhumation of rock through the footwall over time, and should be a function of the amount and rate of displacement both across and along strike of the fault at a first order, modified by any climatically driven variation in exhumation. The amount and rate of displacement along individual normal-faults within developing fault arrays evolves in a predictable manner (e.g., Walsh and Waterson, 1987, 1991; Gupta et al., 1998; Cowie et al., 2000; Trudgill and Cartwright, 1994). Due to the increase in relief and surface-process gradients this spatial distribution of displacement accumulation along an evolving fault array should be manifested in the patterns of footwall exhumation. While many studies have utilized low-temperature thermochronology to determine changes in vertical rates of exhumation, specifically to constrain the onset of rifting (Fitzgerald, 1992; Bauer et al., 2010; Woodruff et al., 2013; Torres Acosta et al., 2015) or to elucidate changes in climatically driven exhumation (e.g., Ehlers et al., 2006; Spiegel et al., 2007), few studies have utilized the technique to determine along-strike fault displacement variations through time. Armstrong et al. (2004) demonstrated a lack of along-strike variation in apatite (U-Th)/He ages (AHe) for the Wasatch fault, USA, such that mechanical segmentation of the fault is not preserved despite its segmented footwall topography. Conversely, Krugh (2008) demonstrated different cooling ages in relay zones that correspond to different timing of mechanical linkage between fault segments along the Wassuk Range in the Basin and Range province, USA.

The lack of thermochronology case studies is surprising as the manner by which extensional fault systems grow is well documented from natural examples and numerical modelling. Normal-faults typically grow through a combination of fault-tip propagation and displacement accumulation, and through fault linkage to produce arrays comprising a series of kinematically linked segments (e.g., Dawers et al.,

1993; Gupta et al., 1998; Cowie et al., 2000). Isolated faults propagate in length as stress builds up at the fault tip; when this overcomes the yield strength of the surrounding rock, it ruptures (e.g., Cowie and Scholz, 1992). As isolated faults propagate toward each other their stress fields interact to produce a feedback effect, whereby the displacement on one structure causes slip on another (Cowie, 1998; Gupta and Scholz, 2000). The anticipated maximum displacement on a single fault is scaled to its overall length (Schlische et al., 1996; Dawers and Anders, 1995). Additionally, the spatial distribution of displacement along strike of individual faults occurs in a relatively predictable pattern due to the mechanisms of fault growth and linkage (Figure 1). Fault-displacement profiles, that is the amount of displacement accumulated across the fault versus distance along strike, of isolated faults have a bell-shaped (often flat topped) profile with the greatest amount of displacement occurring toward the center of a fault and displacement minima at the fault tip (Walsh and Waterson., 1991; Dawers et al., 1993; Cartwright et al., 1995). The idealised displacement profile demonstrated for isolated faults is also documented for evolving fault arrays. Interacting faults achieve a combined displacement for the entire length of the linked array, with maximum displacement in the center and minimum at the tip (e.g., Gupta et al., 1998; Cowie et al., 2000; McLeod et al., 2000). Not all faults achieve this displacement profile through a constant interplay of propagating length and then acquiring displacement. Some isolated segments achieve their length early and then accrue displacement. In this case, fault length is often determined by the interaction with other propagating faults, and structures are initially under-displaced until the bell-shaped profile is achieved (Walsh et al., 2002).

The ideal model of fault interaction (Figure 1) commences with nucleating isolated normal-faults (Cowie, 1992). As these isolated faults propagate they interact

97 with neighboring structures along strike (Cowie et al., 2000). Their fault tips may
98 propagate past one another, and stress builds up within the region of overlapping
99 fault tips; while they are inhibited in lengthening further as the fault tip propagates
100 into the region of reduced stress on the neighboring fault (Gupta and Scholz, 2000).
101 This leads to a steeper displacement gradient close to the overlapping fault tips, and
102 the displacement profile of the individual fault segments becomes asymmetrically
103 skewed toward one another as they interact (Peacock and Sanderson, 1991; Nicol et
104 al., 1996).

105 Instead of continuing to propagate as an isolated fault, the fault segments
106 become mechanically linked across the region of overlap, or “relay” zone to form a
107 single through-going fault, often abandoning the fault tips as the relay is breached
108 (e.g., Walsh and Watterson, 1991; Peacock and Sanderson, 1991; Trudgill and
109 Cartwright, 1994).

110 During this interaction, therefore, the overall length of the fault becomes the
111 combined length of the overlapping fault segments. Where previously there was
112 minimal displacement at the former fault tips, this region is now the center of the
113 through-going fault after linkage. Thus the displacement amount and rate within the
114 relay zone increases as the fault moves towards a bell-shaped displacement profile,
115 with maximum displacement in the center, and minimum at the tip (Gupta et al.,
116 1998). This process can lead to faults appearing to be “under-displaced” in the
117 region of a former relay zone as the amount of displacement in the center adjusts to
118 the new fault length (Gupta et al., 1998). Not all faults will follow this idealised
119 pattern. In the same manner as some fault segments can propagate their length first
120 and later accrue displacement; fault arrays can rapidly acquire their length and
121 subsequently accrue displacement (Morley, 1999).

These patterns of fault growth and linkage should be manifested in AHe dating, as the cooling history along fault strike should vary, reflecting the different rates of displacement accumulation on a propagating normal-fault array.

Here, we apply apatite (U-Th)/He dating to the segmented border fault system of the Karonga Basin of the Malawi Rift, East African Rift System (EARS; Figure 2). The structural evolution of the Karonga Basin is well constrained from previous studies that utilized seismic reflection data (Mortimer et al., 2007). Based upon the distribution of depocenters, the pattern of border fault evolution through the linkage of fault segments, and the presence of a relay zone has been established. Here, we investigate whether this established evolution of the border-fault array is reflected in the footwall AHe cooling ages. Specifically, we aim to determine whether variations in AHe ages exist at similar elevations along-strike, reflecting fault segmentation. In contrast to other studies that have looked to reveal fault segments through AHe analyses, we know the segmentation history and do not rely upon footwall morphology. Instead we evaluate whether the known variations in the spatio-temporal displacement distribution are recorded in the exhumational cooling of the footwall.

2. Geologic setting

The EARS (Figure 2) comprises two geologically distinct, and strongly contrasting branches; the largely amagmatic western and magmatic eastern branches passing either side of the Tanzania Craton, an area of regional doming (Wichura et al., 2015), and superimposed upon existing Proterozoic mobile belts (McConnell, 1972; Shackleton, 1993). The eastern rift is a narrow zone of

146 extensional basins in northern Tanzania and Kenya with well documented spatio-
147 temporal variations in the onset of rift-related volcanism (George et al., 1998;
148 Ebinger and Sleep, 1998; Ebinger, 1989; Morley et al., 1992; Morley, 1999; Michon,
149 2015) that commenced at ca. 43 Ma in Ethiopia. The western rift comprises a series
150 of deep half-graben basins with footwall escarpments rising 1-2 km (Ebinger, 1984,
151 1989; Rosendahl, 1987). The onset of rifting within the western rift varies with the
152 Rukwa Rift initiated 26-25 Ma (Roberts et al., 2012); and <10 Ma in the Albertine
153 graben (Pickford and Senut, 1994), while it has been shown that extension-related
154 exhumation in the Rwzenori Mountains of Uganda began during the Eocene (Bauer
155 et al., 2013). Rifting within the Malawi Rift has previously been considered to have
156 commenced at the onset of volcanism, ca. 8.6 Ma (Ebinger et al., 1993). However,
157 based on apatite fission-track cooling ages, Cenozoic cooling within the Malawi Rift
158 commenced after 40 Ma, with most rapid cooling occurring in the past 20 Ma (van
159 der Beek et al., 1998).

160 The Malawi Rift is in the southernmost rift of the western branch of the EARS
161 and the Karonga Basin refers to the northern lake-filled basin within the rift (Figure
162 2). It is bounded to the east by a large (>90 km long) crustal-scale normal-fault, the
163 Livingstone fault, with >2000 m of footwall relief (relative to lake level); the fault
164 accommodates >4 km of sediments in its hanging wall beneath the deep (up to 600
165 m) Lake Nyasa (Figure 2). The basin fill and border-fault architecture has been well
166 documented from seismic reflection data (Rosendahl, 1987; Ebinger et al., 1993,
167 1987; Scholz, 1989; Mortimer et al., 2007). The sedimentary fill of the hanging wall
168 comprises three depositional sequences (Scholz, 1989; Ebinger et al., 1993;
169 Mortimer et al., 2007): Sequence 1 >8.6 Ma to 2.3 Ma, Sequence 2 from 2.3 Ma to
170 1.6 Ma, and Sequence 3 from 1.6 Ma to present (Ebinger et al., 1993).

The border fault consists of three segments: the northern, central and southern segments (Figure 2). The tips of the central and southern segments overlap where there is a notable step in the shoreline, corresponding to a relay structure, close to the village of Lupingu (red star on Figure 2b). This relay is adjacent to the deepest portion of the modern-day Lake Nyasa. The northern and central segments linked to form a continuous structure early in the basin history, and the corresponding segment boundary is marked by a small step in the lake shoreline (Figure 2; Mortimer et al., 2007). At the top of the Livingstone escarpment is a broad, high-elevation (>2000 m) plateau region (Figure 2).

In addition to the existing seismic studies on the basin, we utilize a reprocessed dataset of the PROBE (Scholz, 1989) survey to better constrain the location of the offshore fault tip of the southern fault segment. A monocline located along strike of the southern segment, with growth strata adjacent to it, pinpoints the location of the fault tip (Figure 2) and defines the 6 km wide relay zone between the two fault segments. This monocline developed late during the deposition of Sequence 2 (post 2.3 Ma), recently in the border-fault evolution. This implies that mechanical linkage occurred relatively recently. Determining the location of the fault tip for the central segment within this relay zone relies upon footwall relief from the SRTM data.

2.1 Evolution of the Livingstone fault

The evolution of the border fault has previously been established (Mortimer et al., 2007; Figure 3). Importantly, at each stage or Sequence of strata in the hanging wall units, the most rapid displacement accumulation is likely to have been located in regions of greatest displacement, identified by regions of greatest sedimentary

thickening (Figure 3b i-iii). Initially, the north and central segments were associated with significant depocenters from Sequence 1 (Figure 3i), and most of the displacement occurred in these regions (Figure 3b i). The central and southern segments were isolated (scenario A in Figure 1), consistent with the onset of rifting occurring earlier in the north than south of the basin (Ebinger et al., 1993; Mortimer et al., 2007). During deposition of Sequence 2 (Figure 3ii) there was a shift in deposition toward the center and south of the basin as these two segments overlapped and the relay zone developed between the central and southern segments. The depocenters associated with the central segment moved toward this relay zone, although the relay was clearly a ramp between the two faults (scenario B in Figure 1). At this time, footwall uplift would have migrated toward the relay zone as displacement skewed (Figure 3ii). The northern segment continued to accrue displacement. During Sequence 3 (Figure 3iii), the relay zone and southern segment are important depocenters, and are regions of highest displacement. The relay zone was breached during the latest stages of Sequence 3 and sediment was deposited into the hanging wall of this breaching fault as the depocenters migrated towards the relay zone (Mortimer et al., 2007). At this time, the fault tip of the central segment was captured into the hanging wall of the through-going fault (scenario C Figure 1). The cumulative displacement along the border fault (Figure 3iv) shows time to basement ranges from 2600 to 4000 ms two-way travel time (twt). Evident from this is the segmentation along the fault that existed during the deposition of Sequence 1. This sequence accrued significant displacement, and combining the total displacement through each stage is still reflected in the cumulative throw today (Figure 3i-iii). The greatest amount of offset of the basement is adjacent to the central segment. The total displacement adjacent to our samples in the northern and

central segments is similar overall. What this cumulative throw does not highlight is that the greatest, and probably most rapid, displacement occurring in the most recent history to the present-day, corresponds to where the lake is deepest (the deepest depocenters being created in the final stages). This is located adjacent to the relay zone and toward the southern segment (Figure 2b). These patterns of fault evolution and hanging wall subsidence can be considered to reflect where the greatest amount and rate of associated footwall uplift and exhumation were likely to have been occurring through time; the depocenter distribution thus can be utilized as a proxy for fault controlled footwall exhumation patterns in the absence of footwall markers for absolute displacement (Figure 3i-iv).

2.2 Existing Low-Temperature Thermochronology

Van der Beek et al. (1998) used apatite fission track (AFT) analyses to investigate the denudational cooling history of the Livingstone escarpment and plateau. The data reveal at least three episodes of cooling and denudation related to regional tectonic events, the most recent in the Cenozoic associated with the present day EARS. AFT ages from the footwall scarp on the central fault segment (the location of the samples of van der Beek et al. (1998) are indicated on Figure 2c) range between 178 and 50 Ma and exhibit a positive age-elevation profile. A single AFT age close to the fault tip and at lake level (460 m; sample DD485a; Figure 1) is 128 Ma; this is anomalously old compared to a sample from the base of the scarp (675 m elevation), which yielded an AFT age of 50 Ma. The data suggest that the center of the fault segment underwent 2.2 ± 0.4 km of exhumation in the Cenozoic, assuming a geothermal gradient of 25-30°C/km. In this study, we aim to determine whether apatite He cooling ages better constrain the evolution of Cenozoic rifting within this region of the Malawi Rift.

3. Apatite He dating Methods

The AHe dating technique relies on the production of alpha particles (^{4}He) as a result of radioactive decay of U, Th and Sm isotopes (Farley et al., 1996). The rate at which He diffuses through a crystal depends on the grain size, time, radiation damage and temperature. Helium starts to be retained within apatite crystals at less than 80°C, with retention increasing dramatically from ~40°C; between ~80 and 40°C is the partial retention zone (PRZ). The AHe ages therefore record the time since these samples were open for He diffusion at temperatures in excess of 40°C. The technique is, therefore, particularly sensitive to processes active in the uppermost part of the crust. We analysed apatites from 10 samples from the region surrounding the relay zone, including two from the summit plateau (TAN 10 and 14), one near the top of the escarpment (TAN 15), four (TAN 16, 17, 18, 20) at, or close to, lake level on the central fault segment, and three (TAN 3, 7, 9) from the northern segment (Figure 2). Apatites were separated using standard heavy-mineral separation techniques. The number of analyses was limited by the quality of the apatite (no inclusions, good crystal morphology) in the samples. Between 1 and 4 aliquots of 1 to 3 apatite grains were hand-picked for each sample at 218x magnification using a stereographic binocular microscope. To minimize grain-size variation effects, crystals of similar radius were selected for each aliquot. He, U and Th analyses were conducted following procedures outlined in Foeken et al. (2006). Correction for He recoil loss was made using standard procedures (Farley and Stockli, 2002). The total analytical uncertainty of He ages of each aliquot is approximately 8%, governed by uncertainty in blank corrections and U and Th spike concentrations. Aliquots that yielded analytical uncertainties greater than 10% (n = 5), and that are older than AFT

ages (n = 5) are not reported. He, U and Th concentrations, grain dimensions, uncorrected ages and corrected ages of our samples are reported in Table 1. Age reproducibility was variable (Table 1), as a result weighted mean ages with appropriate error propagation which takes into account repeat grain-age variance are reported (Table 2) and discussed in the text. The cause of the variability is not clear. Individual samples showed some variation in U and Th content e.g. Tan 14 U: 10-62 ppm; Th: 45-116, whilst others e.g. Tan 16 U: 31-37 ppm; Th: 6.6-7.6 ppm; showed little. As a result effective uranium (eU) ([U] + (0.235*[Th]) which is a proxy for alpha productivity) (Table 1) varies within and between samples, however, there is no systematic correlation between aliquot age and eU content (see Appendix A).

AHe grains were modelled using the HeFTy (v1.8.2) computer program (Ketcham, 2005) using measured U, Th, grain size and uncorrected AHe ages. The time-temperature histories use an inverse modelling approach, for each thermal history the model was constrained by a surface temperature of 20°C and a fission-track age of 50 Ma (DD490; van der Beek et al., 1998); 120 Ma if located in the relay zone or 220 Ma if located on the plateau (DD478; van der Beek et al., 1998). The alpha stopping distance corrections of Ketcham et al. (2011) were used. The calibrations of both Farley (2000) and the radiation damage and annealing model (RDAAM) of Flowers (2009) was implemented, the latter specifically for the samples from the top of the Livingstone plateau, which potentially experienced slow to moderate cooling (1-0.1°C/km). Individual aliquot data were modelled for each sample with the final thermal history profile that is used in the discussion produced to represent the variability of the best fit solutions within the sample set (Figure 4). Overall within sample trends are similar suggesting that despite the age variability, the grains have experienced similar cooling histories.

4. RESULTS: Apatite U/Th-He age distribution.

The lake-level samples between the central and southern segments span 10 km along fault-strike, and there is more than 30 km between these and samples from the northern segment (Figure 2 for location). Samples TAN 17 and TAN 18 are located close to the base of the vertical profile of van der Beek et al. (1998), while the location of sample TAN 16 is is virtually identical to their sample DD485a (AFT age = 128 Ma at 460 m elevation).

The weighted mean AHe ages (Table 2) range from 2.1 ± 1.3 Ma to 197.4 ± 2.7 Ma with the age distribution consistent with the distribution of sampling both along fault strike and from a near-vertical profile from the top of the plateau to the base of the escarpment (Figures 3 and 4). Cenozoic ages occur closest to lake level while the oldest ages (e.g., TAN 10: 197.4 ± 2.7Ma) were determined for samples from the plateau, and at an elevation greater than 1500 m (TAN 14). To the south, the youngest ages are from samples located toward the center of the central fault segment (TAN 17 = 12.5 ± 7.5 Ma and TAN 18 = 7.1 ± 3.2 Ma). TAN 16 (29.7 ± 1.2 Ma), the oldest lake-level sample, is located close to the fault tip. TAN 20 (21.6 ± 9.2 Ma), located within the relay zone and at 673 m elevation, yields a similar age to TAN15 (22.5 ± 3.4 Ma) from the southern segment at 1270 m elevation. The youngest age, TAN 7 (2.1 ± 1.3Ma), is reported from the northern segment, and is considerably younger than the other adjacent Oligo-Miocene ages reported. TAN 3 (14.2 ± 1.1 Ma) is within reported error of TAN 9 (12.1 ± 3.5) close to the center of the northern segment at lake level (Figure 4).

AHe ages not only vary along-strike but also vertically, as shown by the age-elevation relationship (AER; Figure 5). These oldest AHe samples are from the

summit and plateau of the scarp; closer to lake level (460 m) is a spread of younger (Oligo-Miocene) AHe ages (Figure 5). AERs are frequently used to constrain the timing of onset of rapid exhumation or, in this case, the onset of extensional faulting and rift initiation. Given the scatter of Cenozoic ages, care must be taken when considering the AER for the Livingstone escarpment. Samples used for the AER are TAN 14 and TAN 15 that are vertically directly above one another and within the same fault segment, and TAN 20, the closest sample to that profile. There is a distinct break in slope below 1500 m (between TAN 14 and TAN 15) with the AER recording at least one order of magnitude increase in the rate of exhumation. This dramatic change takes place before the late Oligocene/early Miocene (23±3 Ma). This is likely the latest time of onset of Cenozoic exhumation in this part of the Malawi Rift. It is in agreement with the AER from apatite fission-track data that indicated most cooling has occurred in the last 20 million years (van der Beek et al., 1998), and is contemporaneous with the dated onset of Cenozoic rifting in the Rukwa Rift (Roberts et al., 2012) immediately to the north (Figure 2a). This is significantly earlier for the Malawi Rift than has been previously postulated.

The thermal history modelling for all aliquots measured (Figure 4) shows that the samples from the plateau and the top of the footwall escarpment (TAN 10 and TAN 14) experienced slow cooling through the PRZ from the Jurassic. In contrast, samples from the footwall escarpment have all cooled to the surface during the Cenozoic. These samples exhibit somewhat different cooling paths depending upon their position, both vertically and along strike. Samples TAN 15 (1289 m), TAN 16 (560 m, at the fault tip) and TAN 20 (~700 m, southern segment) have similar modelled cooling paths, starting relatively flatter and then steepening slightly as they

343 entered the PRZ between ca.35 and 20 Ma, from which time they cooled relatively
344 monotonically.

345 Samples TAN17 and 18 were exhumed through the PRZ more recently (since
346 c.15 and 9 Ma respectively; Figure 4; Supplementary figure) and more rapidly than
347 other parts of the border fault. This would be anticipated given their position at the
348 center of the fault segment (e.g. Gupta et al., 1998) (Figure 3i-iii). The fact that they
349 do not record their exhumation onset as early as the vertical profile might suggest
350 (i.e., late Oligocene-early Miocene) is potentially due to the greater amount of
351 material that would be exhumed through the central portion of the fault or temporally
352 variable fault-segment activity. Samples TAN 17 and 18 (Figure 4c) record more
353 rapid, tectonically driven exhumation in the past 10 Ma at the center of the structure,
354 as discussed below.

355 From the northern fault segment (Figure 4b), samples TAN 3 and TAN 9 exhibit
356 similar cooling paths; TAN 3 commenced cooling slightly earlier (since c.20 Ma) and
357 more slowly than TAN 9 (since c.15 Ma). These samples are from close to the center
358 of the fault segment, have similar (although later) cooling histories, and are located
359 in a similar position to TAN 18 and TAN 17 in the central fault segment. TAN 7 is
360 exceptionally young (2.1 Ma; Table 2) and may have been reset by hydrothermal
361 fluid flow. Fluid flow was advocated by van der Beek et al. (1998) elsewhere in the
362 rift to explain young AFT ages and this sample is located along a cross-cutting fault
363 (Mortimer et al., 2007) that might explain the fluid pathway. No thermal history
364 models are therefore presented for this sample.

365

366 **5. Discussion**

The new low-temperature cooling ages clearly demonstrate that the fault tip and relay zone (TAN 16, TAN 20) and the northern segment (TAN 3, TAN 9) commenced exhumation in the early Miocene while the center of the southern segment (Tan 17, Tan 18) commenced exhumation more recently. This agrees with the inferred southward propagation rifting within the Malawi Rift (Ebinger et al., 1993). This is consistent with the thicker sediments of the Sequence 1 depocenter adjacent to the northern segment (Figure 3; Mortimer et al., 2007). It is unlikely that ages that record the onset of rifting will be preserved close to lake level as the rapid exhumation associated with fault linkage and changes in displacement rate are probably of greater magnitude than earlier regional uplift associated with Cenozoic rifting. The individual cooling paths are, therefore, more likely to illustrate local changes in displacement rate rather than recording the regional exhumation. The AER shows a break in slope before the Early Miocene (Figure 5) that coincides with the onset of Cenozoic rifting in the Rukwa Rift (Roberts et al., 2012). While this link should be treated with caution, it should also be noted that the cooling ages at the fault tips (which are more likely to preserve regional onset as displacement rates here were lower) are similar, supporting the contention that it does record the timing of onset of *regional* Cenozoic rifting effects in the Malawi Rift.

We consider the variation in AHe ages and cooling paths along the fault segments of the Malawi Rift, in particular the central segment, in the context of the evolution of the border fault system and find their distribution along the fault compelling despite the limited number of data. Rocks closer to the fault tips have experienced a more protracted cooling history than those closer to the segment centers in both the northern and central-southern segments. Additionally, segmentation appears to be preserved along the fault: TAN 16 at the fault tip records

older, more slowly exhumed rocks; despite the present-day scenario of a fully linked, through-going normal-fault bordering an under-filled basin with the maximum displacement at its center (Figure 3; and lake bathymetry, Figure 1).

Within this context, we combine our AHe ages from the Malawi Rift, with the established normal-fault evolution (Mortimer et al., 2007; Figure 3) and predicted models of normal-fault evolution (e.g., Gupta et al., 1998) and envisage the cooling path of rocks at different locations along strike as they are vertically exhumed in an evolving, interacting and linking normal-fault system. This allows us to present a model (Figure 5), focusing upon the relationship between cooling ages along the central and southern segment, but relevant for the northern segment, which not only accounts for the observed AHe age distribution in the Malawi Rift, but also considers the particular scenarios that have led to segmentation being preserved in the cooling paths here.

In a predicted fault profile of displacement along fault strike (*sensu* Gupta et al., 1998), the center of an isolated fault will experience more rapid footwall exhumation than the tip of a fault, as this is where displacement is greatest. Therefore, rocks in the center of the fault segment will begin vertical exhumation earlier and more rapidly than those at the fault tip (Figure 6 a and b; stages 1 and 2).

Faults rarely grow in isolation, but interact along strike leading to a skew in the profile in such a way that the displacement (and exhumation) rate increases toward the overlapping fault and relay zone as the fault segments become linked and effectively become an integral part of the full length of the through-going structure. The central segment is today, mechanically linked to the southern segment across the relay zone. These two segments have interacted and experienced a skew in their

displacement during Sequence 2 and Sequence 3 when depocenters adjacent to the central and southern fault segments moved toward one another and the relay breached toward the end of the time of deposition of Sequence 3 (Mortimer et al., 2007; Figure 3). Rocks being exhumed close to the former fault tips would experience a more rapid cooling later in their history as the new through-going mechanically linked fault develops that is under-displaced in its center (Figure 6 c to d, stages 3 to 4). The skew in displacement profile can also lead to a steepened displacement gradient toward the fault tip (e.g., Nicol et al., 1996). This might explain the different age and cooling paths of TAN 17 and TAN 18 (with TAN 18 located closer to the fault tip accelerating later) and why the fault tip (TAN 16) does not record any acceleration. This suggests that the fault was “under-displaced” (Figure 6 c and d) *sensu* Cartwright et al. (1995). These data are more convincing when considered alongside the existing AFT data (for specific locations see Figure 2), where an anomalously old age for elevation (compared to their vertical profile) of 128 Ma (sample DD485a) is recorded at the fault tip of the central segment. AFT ages from the central fault segment at similar elevations such as DD484 and DD480 exhibit much younger AFT ages (66 and 50 Ma, respectively). This pattern mirrors that of the AHe ages presented here, further supporting the hypothesis that the fault tip (and the relay region) of the central fault segment is preserved in the cooling ages.

The northern and central fault segments are also linked although we do not have the AHe data across this region for comparison. TAN 3 is located closer to the center of the fault segment than TAN 9. In this segment, TAN 9 cooled later and faster than TAN 3, suggesting there was interaction between the northern and central fault segments. The difference in the gradient of the cooling path between TAN 9 and 3

441 (12 km apart) 15 km from the fault tip, compared to TAN 18 and 17 (5 km apart)
442 within 5 km of the fault tip, is possibly related to proximity to the fault tip, as
443 displacement rates increase most rapidly closest to the fault tip during linkage (e.g.,
444 Gupta et al., 1998; Figure 6c).

445 This pattern of increased displacement in the center of the through-going fault
446 has continued along the Malawi Rift into Sequence 3 (Figure 3) where the current
447 subsidence and exhumation are greatest. This region linked during the latest stages
448 of basin evolution, revealed only in the final packages of deposition of Sequence 3,
449 and likely within the past 1 Ma (Mortimer et al., 2007). The relay region remains
450 'under-displaced' and rapidly accrues displacement, leading to a marked increase in
451 exhumation of the footwall as the displacement profile adjusts to the new fault length
452 (Figure 6 e and f; stages 5 and 6).

453 The along-strike age distribution of rocks that have been exhumed to lake level
454 does not reflect the present-day configuration but records earlier fault segmentation.
455 This fault segmentation is preserved in the cumulative throw (time to basement;
456 Figure 2 iv), but is no longer preserved in the footwall profile, or present-day lake
457 bathymetry (Figure 2b). All of these are at their maximum toward the center of the
458 through-going fault adjacent to the relay.

459 Whether or not fault linkage and/or segmentation are likely to be recorded within
460 the distribution of AHe ages along strike is most likely to be related to the timing of
461 mechanical linkage (e.g.,Krugh, 2008), which in the Malawi Rift happened ca.2 Ma
462 (Sequence 3) as demonstrated by the seismic data (Mortimer et al., 2007; Figure 3).
463 Not only is the timing of linkage a factor in recording fault segmentation, but also
464 whether there has been sufficient footwall exhumation to the surface (Figure 6 d-f;

Stages 4-6). Of greatest importance is the appreciation of the lag time between the development of the fault-displacement profile and associated footwall topography and the exhumation of rocks to the surface that record the period of rapid cooling through the PRZ associated with this increased displacement rate.

Our data in the Malawi Rift, preserve a snapshot of tectonically driven exhumation in which the segmentation is preserved. Beneath the lake surface is an inaccessible 600 m fault scarp. Somewhere along this structure the rocks that record accelerated cooling associated with linkage at ~1.6 Ma have yet to be exhumed to lake level. Van der Beek et al. (1998) utilized a geothermal gradient of 25-30°C/km based on estimates of heat flow in a regional study by Nyblade et al. (1990). Given this geothermal gradient, any samples experiencing a more rapid exhumation since ~ 1.6 Ma would still be ~1 km below the surface; or, with a slightly greater gradient, at lake bed, but still >500m below lake level. Therefore, samples at or above lake-level today should reflect the fault configuration from Sequence 1 and Sequence 2, as rocks cooled through the PRZ, from the later stages of Sequence 2 and Sequence 3 have not yet been exhumed to the surface (Figure 6e; stage 5). Thus, our ages should reflect fault interaction but not the present-day, more rapid displacement accumulation adjacent to the relay, as is the case. AHe ages lower within the footwall would reflect the most recent cooling history and eventually ages along-strike would no longer record the fault segmentation but represent a single through-going structure (Figure 6f). This is perhaps the end-member scenario represented by the history of the Wasatch fault in Utah (Armstrong et al., 2004), where there is no record of separate segments preserved within AHe ages. As suggested by Krugh (2008), different cooling ages in relays along a fault array are determined by when mechanical linkage occurs. The exhumation or preservation of

fault segmentation within the footwall rocks is controlled by the timing of mechanical linkage, the geothermal gradient, and rates of displacement across the fault. In the Malawi Rift, we are fortunate that the interplay of these parameters has led to the preservation of the record of segmentation.

To thoroughly reveal the fault-segment history would require a rigorous series of horizontal and vertical transects across the footwall that mimic the type of investigation provided by stratigraphic interpretations of a hanging wall. Nonetheless, changes in the rate of vertical exhumation due to the pattern of fault growth and linkage should be thoroughly evaluated if a single vertical profile is being used to determine variations in external driving forces such as climate or the onset of rifting.

6. Conclusions

The age-elevation relationship of our data from the Livingstone fault, Malawi, shows that important, regional-scale cooling associated with Cenozoic rifting commenced at ~23 Ma, slightly later than the Rukwa Rift to the north. This is significantly earlier than the onset of volcanics (Ebinger et al., 1993) and previously proposed rift onset; but is in agreement with proposed rapid Cenozoic exhumation since ca. 20 Ma based upon existing AFT cooling ages (van der Beek et al., 1998).

Our data show that low-temperature (AHe) thermochronology does record segmentation of the Livingstone border fault, Malawi. This fault segmentation is recorded by along-strike variations in AHe ages that show protracted cooling at palaeo-fault tips, and more rapid cooling toward the center of active fault segments.

512 The AHe age distribution does not reflect the present-day fault configuration of
513 the Livingstone fault, which experiences the maximum displacement in and close to
514 the relay zone, but instead records the fault segmentation from earlier in the basin
515 history.

516 There is a significant lag between fault interaction, linkage, rapid uplift at any
517 given location, and the vertical exhumation of rocks from the PRZ to lake-level that
518 reflect that interaction. The relatively recent linkage (~1.6 Ma) of the central and
519 southern segments of the Livingstone fault emphasizes that older fault segmentation
520 is more likely to be preserved than in older linked systems.

521

522 **7. ACKNOWLEDGEMENTS**

523 The authors thank Peter van der Beek for providing AFT data, and many
524 constructive discussions; Rasmus Thiede for everything while in the field in
525 Tanzania; Evelyne Mbede, for so many insights and guidance on sampling locations;
526 Mr Songo for field assistance; David Vilbert for running analyses and Jurgen Foeken
527 for analyses and discussion at SUERC. Funding for fieldwork, and analyses were
528 provided to M.R. Strecker by DFG (Deutsche Forschungsgemeinschaft) grants STR
529 373/15-1 and 19-1. We would like to thank Chris Morley and an anonymous reviewer
530 for their constructive comments.

531

532 **REFERENCES**

533 Armstrong, P.A., Taylor, A.R., Ehlers, T.A., 2004, Is the Wasatch fault footwall (Utah,
534 United States) segmented over million-year time scales?: Geology, 32, 385–388.

535 Bauer, F.U., Glasmacher, U.A., Ring, U., Schumann, A., Nagudi, B., 2010, Thermal
536 and exhumation history of the central Rwenzori Mountains, Western Rift of the East
537 African Rift System, Uganda: International Journal of Earth Science (Geol
538 Rundsch), 99, 1575–1597.

539 Cartwright, J.A., Trudgill, B.D., Mansfield, C.S., 1995, Fault growth by segment
540 linkage: an explanation for scatter in maximum displacement and trace length data
541 from the Canyonlands Grabens of SE Utah: Journal of Structural Geology, 17, 1319-
542 1326.

543 Cowie, P.A., 1998, A healing-reloading feedback control on the growth rate of
544 seismogenic faults: Journal of Structural Geology, 20, 1075-1087.

545 Cowie, P.A., and Scholz, C.H., 1992, Displacement-length scaling relationship for
546 faults: data synthesis and discussion: Journal of Structural Geology, 14, 1149-1156.

547 Cowie, P.A., Gupta, S., Dawers, N.H., 2000, Implications of fault array evolution for
548 syn-rift depocenter development: insights from a numerical fault-growth model: Basin
549 Research, 12, 241-261.

550 Dawers, N.H., and Anders, M.H., 1995, Displacement-length scaling and fault
551 linkage: Journal of Structural Geology, 17, 611-614.

552 Dawers, N.H., Anders, M.H., Scholz, C.H., 1993, Growth of normal-faults:
553 Displacement-length scaling: Geology, 21, 1107-1110.

554 Ebinger, C.J., 1989, Tectonic development of the western branch of the East African
555 rift system: Geological Society of America Bulletin, 101, 885-903.

556 Ebinger, C., M. Crow, B. Rosendahl, D. Livingstone, and J. Le Fournier, 1984,
557 Structural evolution of the Malawi rift, Africa: Nature, 308, 627-629.

558 Ebinger, C. J., and Sleep, N.H., 1998, Cenozoic magmatism throughout east Africa
559 resulting from impact of a single plume: Nature, 395, 788-791.

560 Ebinger, C. J., Deino, A. L., Tesha, A. L., Becker, T: & Ring, U., 1993, Tectonic
561 controls on rift basin morphology: evolution of the Northern Malawi (Nyasa) rift:
562 Journal of Geophysical Research, 98, 17821-17836.

563 Ehlers T.A., Farley K.A., Rusmore M.E., Woodsworth G.J., 2006, Apatite (U-Th)/He
564 signal of large magnitude and accelerated glacial erosion: southwest British
565 Columbia: Geology, 34, 765– 768, doi: 10.1130/G22507.1.

566 Farley, K.A., 2000 Helium diffusion from apatite: general behaviour as illustrated by
567 Durango flourapatite: Journal of Geophysical Research B, 105, 2903-2914.

568 Farley, K.A., and Stockli D.F., 2002, (U/Th)/He dating of phosphates: Apatite,
569 monzanite and xenotime *in* Kohn, M et al., eds., Phosphates-Geochemical,
570 geobiological and material imporTANce: Mineralogical Society of America Reviews
571 in Mineralogy and Geochemistry, 48, 557-577.

572 Farley, K.A., Wolf, R.A., and Silver, L.T., 1996, The effects of long alpha-stopping
573 distances on (U-Th)/He ages: Geochimica et Cosmochimica Acta, 60, 4223-4229.

574 Fitzgerald, P. G. (1992), The Transantarctic Mountains of southern Victoria Land:
575 The application of apatite fission track analysis to a rift shoulder uplift, Tectonics, 11,
576 634–662, doi:10.1029/91TC02495.

577 Flowers, R.M., 2009, Exploiting radiation damage control on apatite (U–Th)/He dates
578 in cratonic regions: Earth and Planetary Science Letters, 277, 148-155.

579 Foeken, J.P.T., Stuart, F.M., Dobson, K.J., Persano, C.P., and Vilbert, D., 2006, A
580 diode laser system for heating minerals for (U-Th)/He chronometry: Geochemistry,
581 Geophysics, Geosystems, v. 7, DOI: 10.1029/2005GC001190

582 George, R., Rogers, N., and Kelley, S., 1998, Earliest magmatism in Ethiopia:
583 Evidence for two mantle plumes in one flood basalt province: Geology, 26, 923-926.

584 Gupta, S., Cowie, P.A., Dawers, N.H, & Underhill, J.R., 1998, A mechanism to
585 explain rift-basin subsidence and stratigraphic patterns through fault array evolution:
586 Geology, 26, 595-598.

587 Gupta, A., and Scholz, C. H., 2000, A model of normal-fault interaction based on
588 observations and theory, Journal of Structural Geology, 22**,** 865–879.

589 Jackson, J., and McKenzie, D., 1983, The geometrical evolution of normal fault
590 systems: Journal of Structural Geology, 5, 471-482.

591 Ketcham, R., 2005, Forward and inverse modeling of low temperature
592 thermochronometry data: *in* Reiners, P.W., and Ehlers, T.A., eds., Low-temperature
593 thermochronology: Techniques, interpretations and applications: Reviews in
594 Mineralogy and Geochemistry, 58, 275-314.

595 Ketcham, R.A., Gautheron, C., and Tassan-Got, L., 2011, Accounting for long alpha-
596 particle stopping distances in (U‐Th‐Sm)/He geochronology: Refinement of the
597 baseline case: Geochimica et Cosmochimica Acta, 75, 7779-7791.

598 Krugh, W.C., 2008, Low-temperature thermochronologic constraints on fault array
599 evolution and patterns of range-scale denudation: *PhD Thesis,* ETH, Zurich (2008).

600 McConnell, R.,1972, Geological development of the rift system of East Africa: GSA
601 Bulletin, 83(9), 2549–2572, doi:10.1144/gsl.sp.1978.006.01.04.

602 Michon, L., 2015, What the volcanism of the East African Rift tells us on its evolution
603 and dynamics: a reappraisal: Geophysical Research Abstracts, 17, EGU2015-3407.

604 Morley C.K., Wescott W.A., Stone D.M., Harper R.M., Wigger S.T. & Karanja F.M.,
605 1992, Tectonic evolution of the northern Kenyan Rift: Journal of the Geological
606 Society of London, 149, 333-348.

607 Morley, C.K., 1999, Patterns of displacement along large normal-faults: Implications
608 for basin evolution and fault propagation based on examples from East Africa: AAPG
609 Bulletin, 83, No 4, 613-634.

610 Mortimer, E.J., Paton, D.A., Scholz, C.A., Strecker, M.R., and Blisniuk, P., 2007,
611 Orthogonal to oblique rifting: effect of rift basin orientation in the evolution of the
612 North basin, Malawi Rift, East Africa: Basin Research, 19, 393-407.

613 McLeod, A.E., Dawers, N.H., and Underhill, J.R., 2000, The propagation and linkage
614 of normal-faults: insights from the Strathspey-Brent-Statfjord fault array, northern
615 North Sea: Basin Research, 12, 263-284.

616 Nyblade, A.A., Pollack, H.N., Jones, D.L., Podmore, F., and Musjayandebvu, M.,
617 1990, Terrestrial heat flow in East and Southern Africa: Journal of Geophysical
618 Research, 95, 17,371-17,384.

619 Peacock, D,C,P, and Sanderson, D.J., 1991, Displacements, segment linkage and
620 relay ramps in normal-fault zones: Journal of Structural Geology, 13, 721-733.

621 Pickford, M., and B. Senut, 1994, Palaeobiology of the Albertine Rift Valley: General
622 conclusions and synthesis, in Geology and palaeobiology of the Albertine Rift Valley,
623 Uganda-Zaire, edited by B. Senut and M. Pickford, pp. 409–423, CIFEG Occasional
624 Publication, Orléans.

625 Roberts, E.M., Stevens, N.J, O'Connor, P.M., Dirks P.H.G.M., Gottfried, W.C., Clyde,
626 W.C., Armstrong, R.A., Kemp, A.I.S., Hemming, S., 2012, Initiation of the western
627 branch of the East African Rift coeval with the eastern branch: Nature, 5, 289-294.

628 Rosendahl, B. R., 1987, Architecture of continental rifts with special reference to
629 East Africa: Annual Review Earth and Planetary Science, 15, 445-503.

630 Scholz C.A, 1989, Project PROBE geophysical atlas series, Duke University,
631 Durham, N. Carolina.

632 Schlische, R.W., Young, S.S., Ackermann, R.V., Gupta, A., 1996, Geometry adn
633 scaling relations of a population of very small rift-related normal-faults: Geology, 24,
634 683-686.

635 Shackleton R.M., 1993, Tectonics of Mozambique Belt in East Africa. In: Prichard
636 H.M., Alabaster T., Harris N.B.W & Neary C.R E (Eds), Magmatic Processes and
637 Plate Tectonics. Geol. Soc. Spec. Publ., 76, 345-362.

638 Stein, R.S. and Barrientos, S.E., 1985, Planar High-Angle faulting in the Basin and
639 Range: Geodetic analysis of the 1983 Borah peak, Idaho, Earthquake: Journal of
640 Geophysical Research, 90, 11355-11366.

641 Trudgill, B., and Cartwright, J.A., 1994, Relay-ramp forms and normal-fault linkages,
642 Canyonlands National Parl, Utah: GSA Bulletin., 106, 1143-1157.

643 Van der Beek, P., Mbede, E., Andriessen, P.A.M., Delvaux, D., 1998, Denudation
644 history of the Malawi and Rukwa Rift flanks (East African Rift System) from apatite
645 fission track thermochronology: Journal of African Earth Sciences, 26, 363-385.

646 Walsh, J.J., and Watterson, J., 1987, Distribution of cumulative displacement and
647 seismic slip on a single normal-fault surface, Journal of Structural Geology, 9, 1039-
648 1046.

649 Walsh, J.J., and Watterson, J., 1991, Geometric and kinematic coherence and scale
650 effects in normal-faults systems. In: The Geometry of Normal-faults, Roberts A.M.,
651 Yeilding, G., and Freeman, B (Eds): Geological Society Special Publication, 56, 193-
652 203

653 Walsh, J.J., Nicol, A. and Childs, C., 2002, An alternative model for the growth of
654 faults: Journal of Structural Geology, 24, 1669-1675.

655 Wichura, H., Jacobs, L. L., Lin, A., Polcyn, M. J., Manthi, F. K., Winkler, D. A.,
656 Strecker, M. R. and Clemens, M, 2015, A 17-My-old whale constrains the onset of
657 uplift and climate change in east Africa, Proc. Natl. Acad. Sci. U.S.A., 112(13),
658 3910–3915, doi:10.1073/pnas.1421502112.

659 Woodruff, W.H., Horton, B.K., Kapp, P., and Stockli, D.F., 2013, Late Cenozoic
660 evolution of the Lunggar extensional basin, Tibet: Implications for basin growth and
661 exhumation in hinterland plateaus: GSA Bulletin, 125, 343-358.

662

663 **Figure Captions**

664 **Figure 1**: Growth and linkage of normal-faults and the predicted corresponding along
665 strike displacement accumulation. The displacement profile is the amount of
666 displacement, D, measured along fault strike, X. The idealised displacement profile
667 for a normal-fault is a bell shaped curve with maximum displacement in the center
668 and zero at the fault tip, such as in A. As two faults propagate toward each other,
669 their tips can overlap (overlapping faults, B), forming a relay ramp. Their stress fields
670 interact and displacement on each fault segment is skewed toward the center of the
671 overlap. Finally, the faults become linked as the relay ramp is breached (C) and the
672 fault is initially under-displaced in the center (compared to an idealised profile). Post
673 linkage displacement is, therefore, greatest in the center of the linked fault, where
674 previously the tips overlapped (B and C are modified from Trudgill and Cartwright,
675 1994).

676 **Figure 2**: (a) Location of the North Basin, Malawi Rift (study area in red box) as the
677 southernmost rift basin of the western branch of the EARS. The northern two thirds
678 of the Malawi Rift are filled by Lake Nyasa, which reaches up to 800 m depth at its
679 deepest portion. We investigate the northernmost basin, the Karonga Basin, of the
680 Malawi Rift. (b) AHe samples (yellow circles) are from the northern segment (TAN03,
681 07 and 09) and from central and southern segment relay zone (enlarged in d) by the
682 village of Lupingu (red star). The present day bathymetry (cool colours deep and
683 warm colours shallow) is deepest adjacent to the relay zone and the southern
684 segment. (c) Enlargement of the relay zone showing the location of AFT samples of
685 van der Beek et al., 1995 (blue circles), and their spatial relationship to our samples.
686 Those labelled are referred to in the text. d.) The Livingstone Escarpment looking

687 from the north of the lake along the northern segment of the border fault system.
688 Samples TAN03, 09, 07 are located along this segment.

689 **Figure 3:** Known evolution of the border fault system (modified after Mortimer et al.,
690 2007). The locations of our samples (yellow circles), and the village of Lupingu (red
691 star) within the relay zone are indicated. a. (i-iii) Isopach (thickness in ms two-way-
692 time) maps for sedimentary sequences and (iv) depth to basement, adjacent to the
693 border fault. b. The evolution of the segmented border fault system with regions of
694 greatest displacement rate, and therefore most likely to experience rapid exhumation
695 indicated (yellow arrows with size reflecting envisaged difference in rates - large fast,
696 small slower) along the segments. These patterns of exhumation and fault
697 segmentation should be reflected in the thermal evolution of the footwall.

698

699 (i) Sequence 1: the northern segment and northern portion of the central segment
700 experienced the most displacement, in particular adjacent to TAN03, 07 and 09;
701 while to the south along the central and southern segments there was significantly
702 less displacement (TAN17, 18 and 20). The south segment fault tip had not
703 propagated into the relay zone at this time.

704 (ii) Sequence 2: the southern segment and central segment are more active,
705 displacement increased adjacent to TAN17 and 18, as the depocenter moved toward
706 the south and the fault tips had propagated past one another.

707 (iii) Sequence 3: the most recent, is a thin succession with a delta entering the
708 under-filled lake from the north, with much sedimentation focussed adjacent to the
709 relay zone. TAN16 and 20 are within the region of overlap between these two fault

segments. As the relay structure was breached by a fault (final stages of Sequence 3; Mortimer et al., 2007) sediments accumulate in the hanging wall. TAN16 and 20 are captured into the footwall of this breached relay as the fault tip of the central segment is abandoned, while TAN17 and 18 remain along the central segment footwall.

(iv) two-way-time to basement: is the cumulative effect that encompasses all of the fault displacement that has occurred between rift onset and the present day. The cumulative throw is similar in distribution to Sequence 1 and preserves the fault segmentation. This shows that the greatest cumulative displacement is adjacent to the central fault segment. However, this does not reveal where displacement rates are greatest today - adjacent to the relay and southern segments, as shown by the bathymetry of the lake bed (see Figure 2).

Figure 4: Results of the modelled cooling path of each sample using the HeFTy computer program (Ketcham, 2005). Samples were modelled with each grain independently, and the cooling paths for individual grains are shown for each sample (solid black lines). Each different portion of the fault array investigated is represented separately to relate the cooling paths to the position of the sample both vertically and along fault strike.

The location of samples are shown with (a.) the plateau region (purple); (b.) the northern segment of the Livingstone fault (green) and (c.) the central-south segments including the relay zone in (red for at or close to lake level; orange for escarpment samples). The distribution of AHe ages for each sample is shown in bold (2 sigma errors in brackets) adjacent to the sample location on the maps.

Figure 5: Age-Elevation relationship (AER) of samples (weighted mean age) from the Livingstone escarpment (see Figure 1 for location). Samples may be considered relating to their position along strike and vertically within the fault array by the following: Livingstone plateau and summit (diamond); northern segment (squares); southern and central segments and the relay zone (triangles). Vertical AER (grey line on graph) and located on the inset (yellow line) through samples close to the fault tip (TAN20), the escarpment (TAN15) and plateau (TAN14). Summit sample TAN10 is considerably further along strike on the plateau (Figure 1). The wide range of ages at or close to lake level is likely to be associated with differing displacement rates along fault strike, see text for discussion.

Figure 6: Envisaged tectonically driven vertical cooling paths of rocks through the Partial Retention Zone (PRZ) resulting from footwall uplift and exhumation (grey shading) associated with normal-fault displacement (D). Patterns of footwall exhumation change as two fault segment link to become a single through-going fault. Rocks that enter the PRZ at the same time are represented by dots of the same colour (t=0 to t=6; stages 1-6). Spatio-temporal variations in tectonically driven exhumation lead to rocks of the same cooling age reaching the surface at different times. Each figure shows the cooling path of rock through the PRZ corresponding to the evolution of the displacement profile along the fault.

The along-strike lake-level age distribution (coloured dots along lake-level; stages 4-6) will at times reflect earlier fault segmentation with older ages in the center of the linked array (stage 4 and 5), despite the footwall topography corresponding to a single through-going fault.

Eventually, sufficient exhumation occurs and segmentation is no longer recorded at lake-level, and rapid exhumation in the center corresponds to the youngest ages exhumed. We envisage a Stage 5 scenario for the Malawi Rift, where linkage occurred too recently (~2 Ma) for samples whose cooling path records the present day displacement to have been exhumed to lake-level.

Figure 1 low res

Click here to download high resolution image

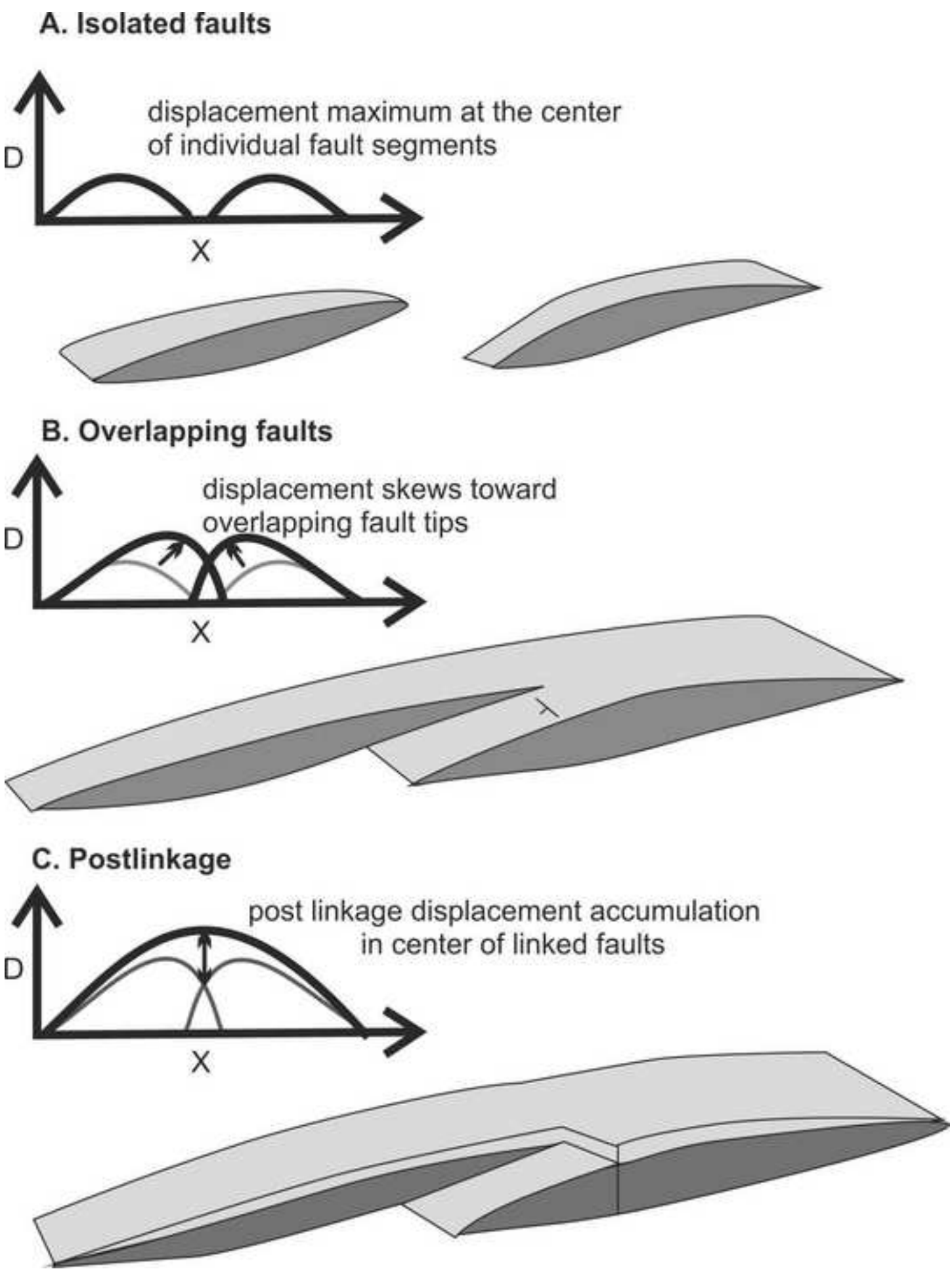

Figure 2 low res

Click here to download high resolution image

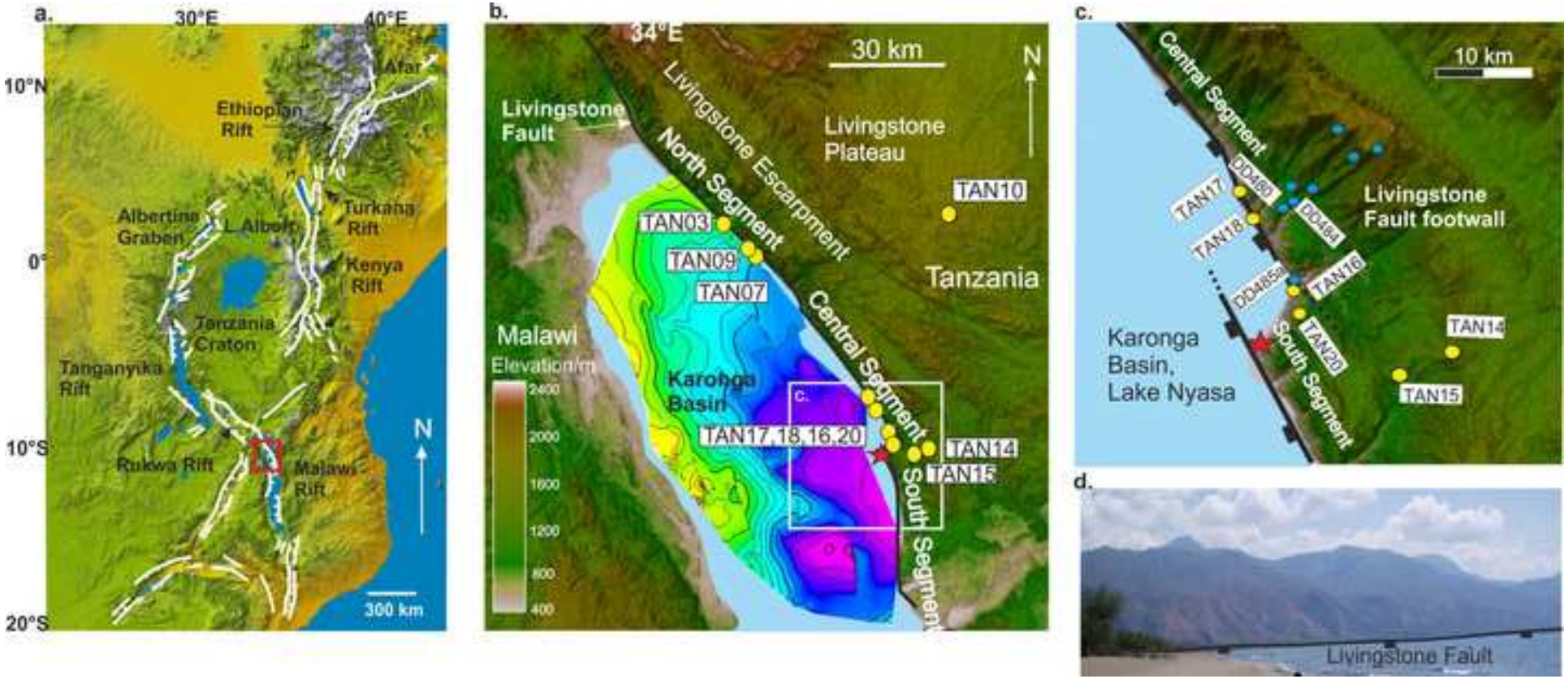

Figure 3 low res

Click here to download high resolution image

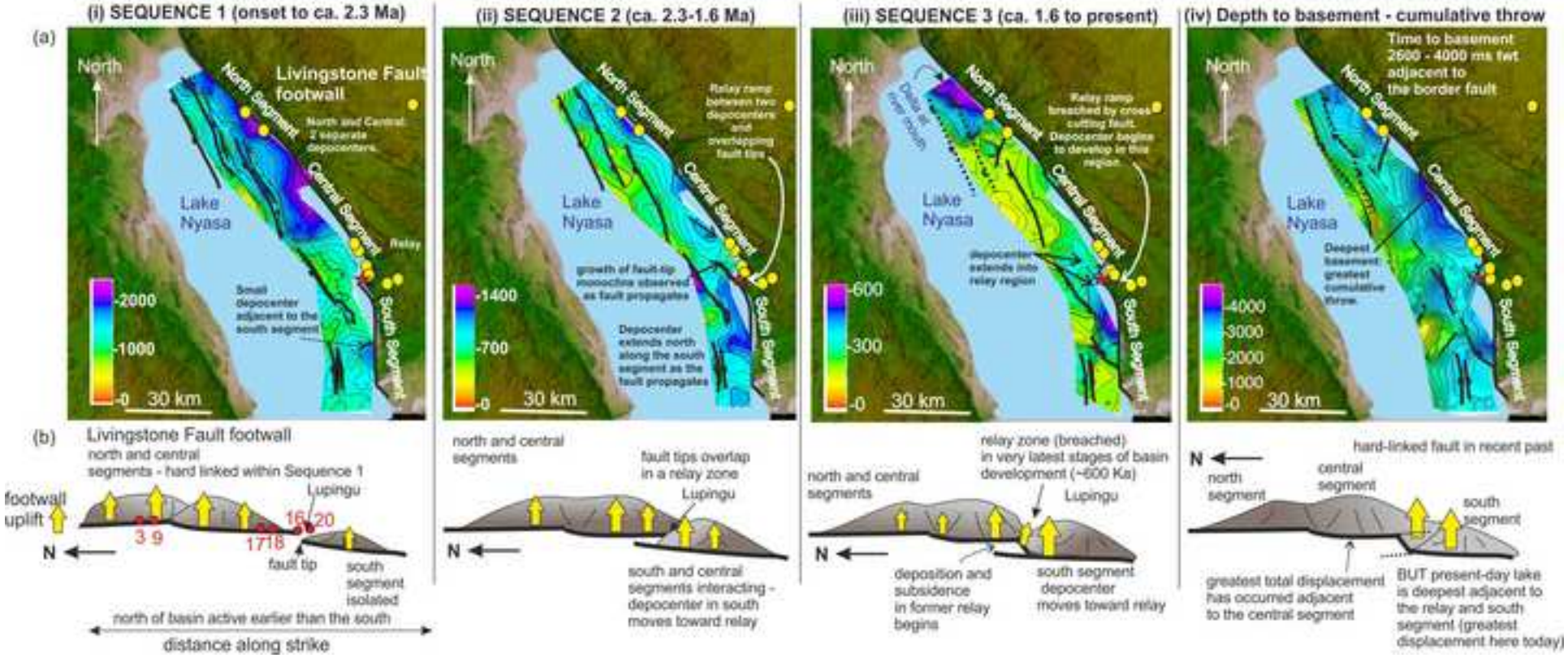

Figure 4 low res

Click here to download high resolution image

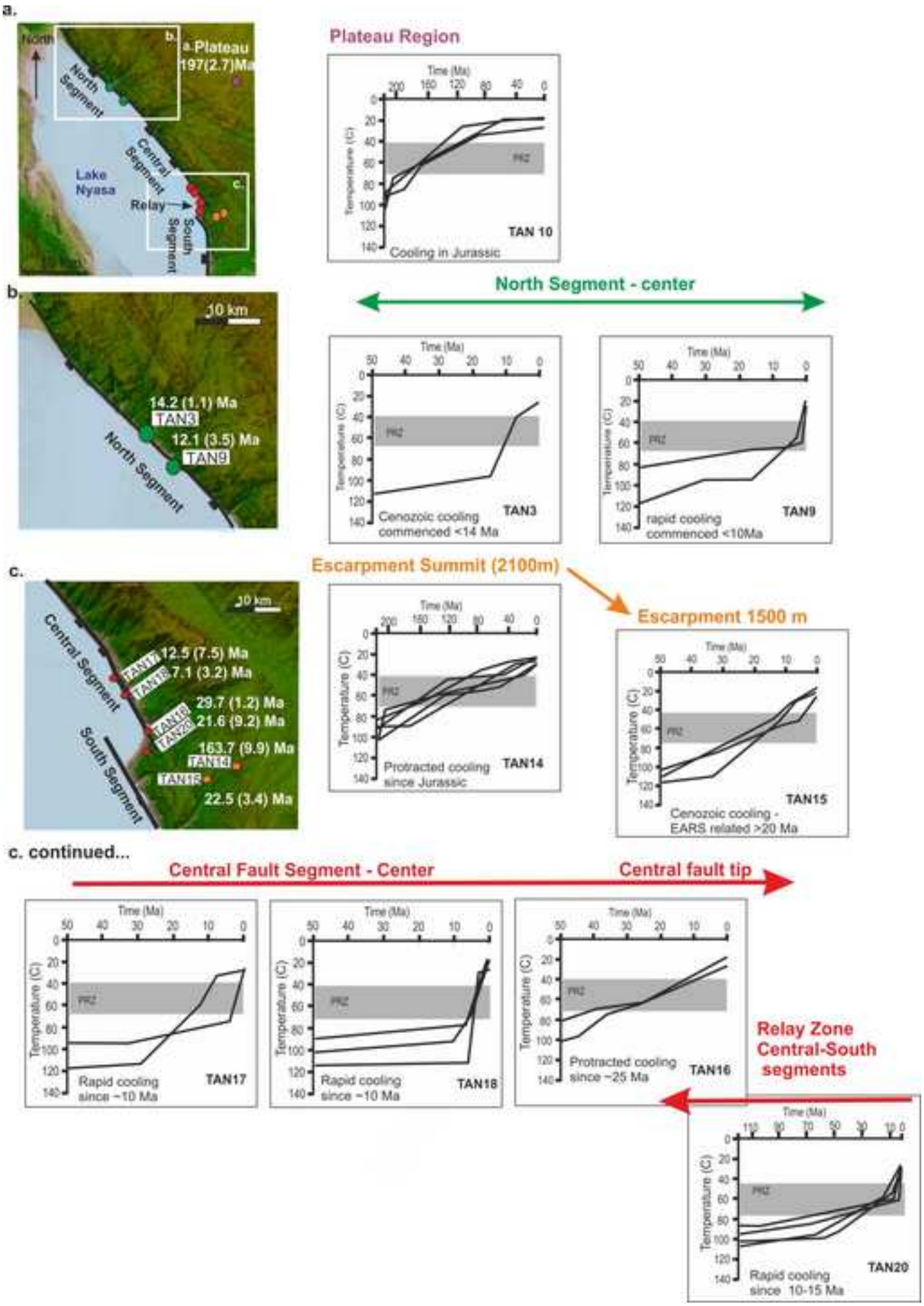

Figure 5 low res

Click here to download high resolution image

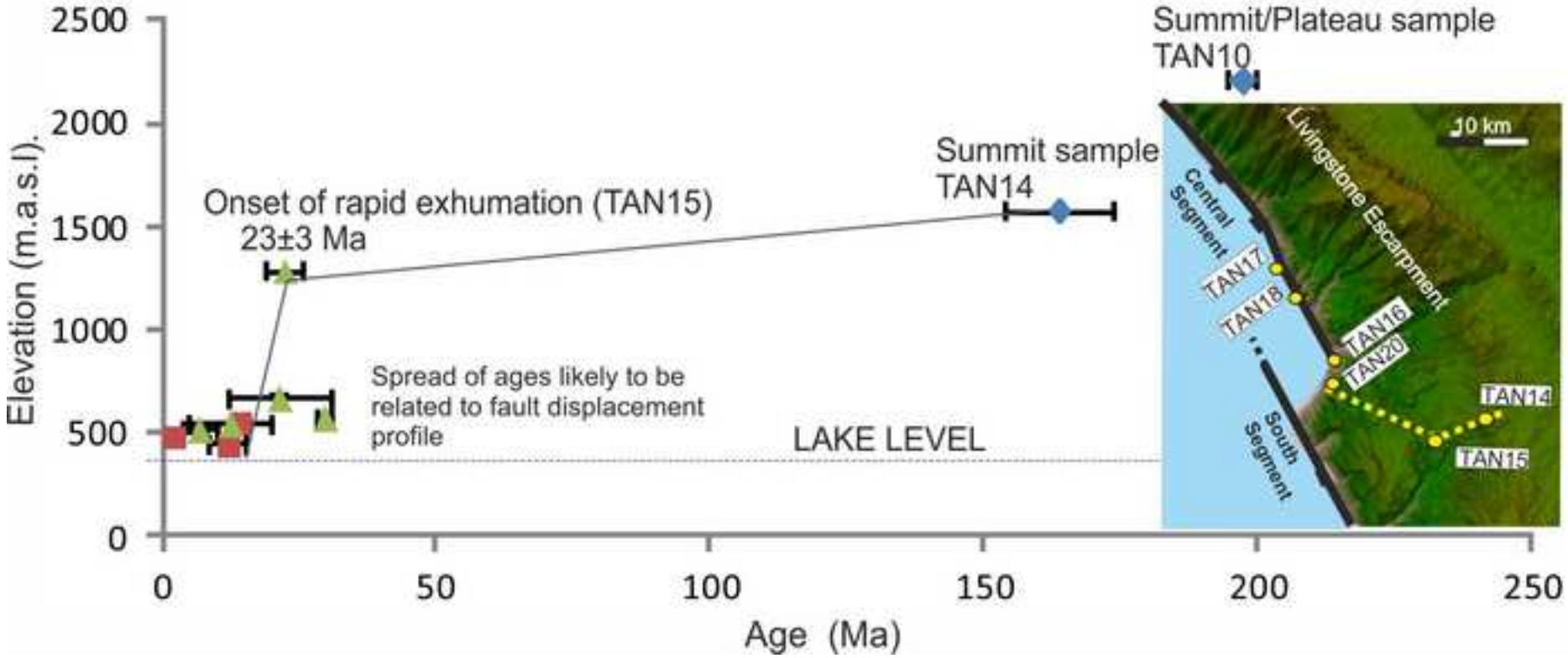

Figure 6 low res

Click here to download high resolution image

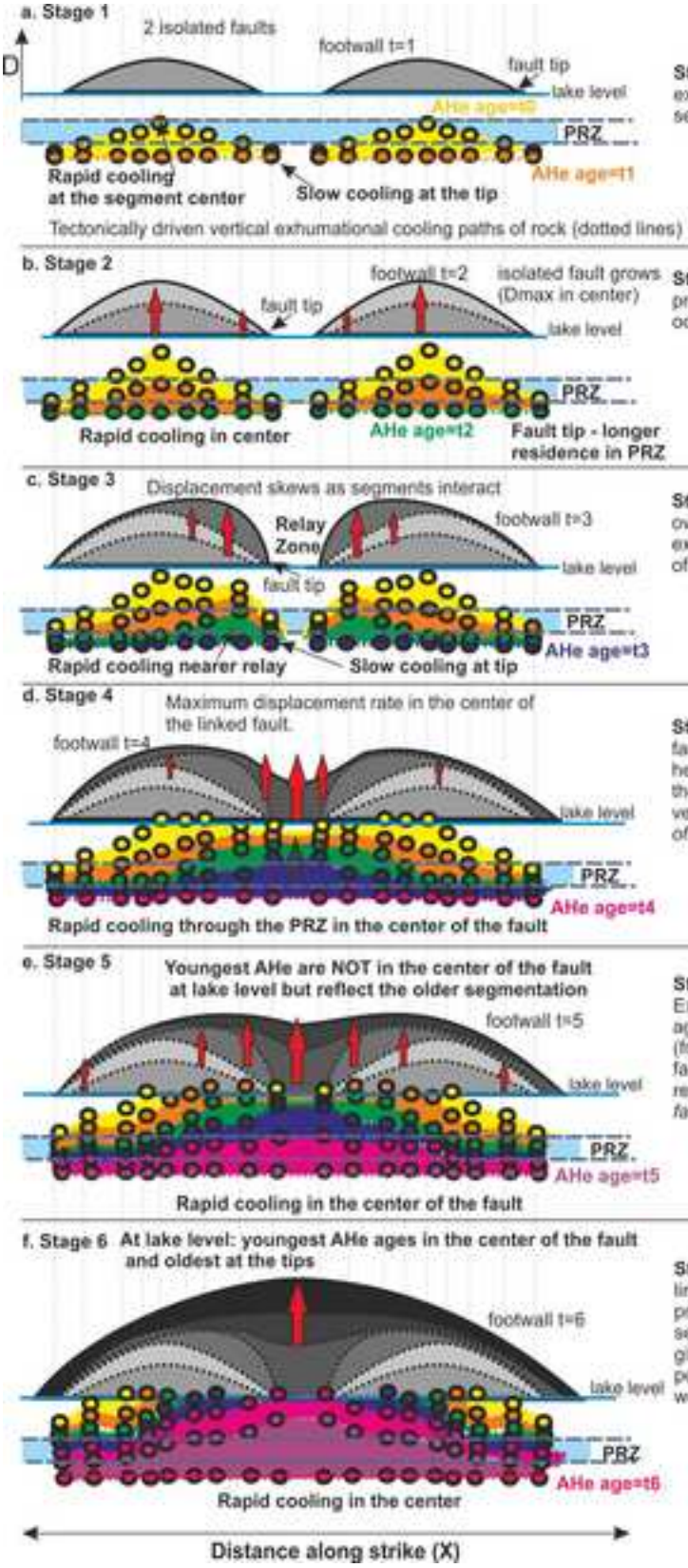

Stage 1: Isolated structures with rocks in the center of the segments being exhumed most rapidly. Leads to more rapid cooling through the PRZ in the segment center.

Stage 2: Isolated structures continue to evolve. Cooling at the fault tip is more protracted than at the center of individual segments. Most rapid exhumation occurs in the center

Stage 3: En echelon fault segments interact. Displacement skews to the overlapping fault tip. Cooling becomes more rapid toward that fault tip, exhumation continues in the center but is relatively less than toward the region of overlap. At the far fault tips cooling is still protracted.

Stage 4: Linkage occurs, displacement is greatest in the center of the linked fault segments as the "under-displaced" fault adjusts. Rapid cooling occurs here, but exhumation continues along the length of the fault bringing rocks to the surface. Samples reflecting rift onset would now be at lake level in any vertical profile undertaken in the center of a fault segment *but not in the center of the linked fault.*

Stage 5: Increased displacement occurs in the center of the linked fault. Exhumation is rapid, while cooling at the tips remains more protracted. AHe age distribution along strike preserves fault segmentation, with the oldest ages (from a time of more protracted cooling) occurring to the center of the linked fault and younger ages toward the center of each segment. This pattern of ages reveals the segmentation *despite the footwall morphology reflecting a single fault.* ***We envisage this scenario to explain the Malawi Rift data.***

Stage 6: Rapid displacement continues to be focussed in the center of the linked fault. Exhumation is rapid here, while cooling at the tips remains more protracted. AHe age distribution along strike no longer preserves fault segmentation. Youngest AHe ages are in the center of the linked fault. In any given vertical profile, however, the onset of protracted cooling (and therefore potentially interpreted as rift onset or invoked climate or other driving changes) would vary significantly.

Table 1

Click here to download Table: mortimer et al table 1.docx

Sample name	Northing	Easting	^{4}He (ccSTP)	^{238}U (ng)	^{235}U (ng)	^{232}Th (ng)	Th/U	error	Uncorr. He age (Ma)	Ft	Corr. He age (Ma)	Error (Ma)	Blank Used
Livingstone summit and plateau.													
TAN 10-1	8942252	684162	6.048E-09	0.215	0.002	0.573	2.7	0.0	140.7	0.71	197.0	4.5	CT DUR
TAN 10-2	8942252	684162	8.320E-09	0.298	0.002	0.576	1.9	0.0	155.9	0.80	195.9	4.4	CT DUR
TAN 10-3	8942252	684162	2.043E-08	0.646	0.005	1.757	2.7	0.0	156.9	0.79	199.5	4.7	CT DUR
TAN 14-1a	8881903	679108	7.858E-09	0.285	0.002	0.868	3.0	0.0	130.8	0.85	154.5	6.9	VU DUR
TAN 14-1b	8881903	679108	4.251E-09	0.105	0.001	0.592	5.6	0.1	141.9	0.86	164.4	7.5	VU DUR
TAN 14-1c	8881903	679108	5.120E-09	0.176	0.001	0.530	3.0	0.0	138.8	0.83	166.8	7.0	VU DUR
TAN 14-2	8881903	679108	1.376E-08	0.633	0.005	1.161	1.8	0.0	123.7	0.82	150.0	6.6	VU DUR
TAN 14-3	8881903	679108	3.957E-09	0.133	0.001	0.453	3.4	0.1	134.5	0.76	176.4	5.4	VU DUR
Livingstone Fault escarpment (North segment)													
TAN 03-A	8940289	626406	7.652E-11	0.029	0.000	0.094	3.3	0.1	12.4	0.87	14.2	0.3	VU DUR
TAN 05	8946770	617979	1.074E-09	0.051	0.000	0.111	2.2	0.0	113.2	0.69	163.6	5.1	VU DUR
TAN 07-A	8931423	634768	6.784E-12	0.056	0.000	0.267	4.8	0.1	0.5	0.67	0.7	0.0	VU DUR
TAN 07-B	8931423	634768	1.609E-11	0.043	0.000	0.162	3.7	0.1	1.6	0.77	2.1	0.1	VU DUR
TAN 07-C	8931423	634768	1.587E-11	0.062	0.000	0.287	4.6	0.1	1.0	0.66	1.5	0.0	VU DUR
TAN 09-A	8933587	632621	3.647E-11	0.030	0.000	0.026	0.9	0.0	8.3	0.74	11.2	0.3	VU DUR
TAN 09-C	8933587	632621	4.195E-11	0.030	0.000	0.016	0.5	0.0	10.1	0.69	14.7	0.5	VU DUR
Livingstone Fault escarpment (North segment)													
TAN 15-A	8880090	676027	1.853E-10	0.073	0.001	0.058	0.8	0.0	17.5	0.82	21.5	0.5	VU DUR
TAN 15-B	8880090	676027	1.714E-10	0.077	0.001	0.041	0.5	0.0	16.2	0.75	21.5	0.6	VU DUR
TAN 15-C	8880090	676027	1.833E-10	0.065	0.000	0.048	0.7	0.0	19.7	0.77	25.6	0.7	VU DUR
TAN 20-A	8885312	669333	7.835E-10	0.227	0.002	0.204	0.9	0.0	23.4	0.77	30.3	0.7	VU DUR
TAN 20-B	8885312	669333	1.405E-09	0.610	0.004	0.344	0.6	0.0	16.7	0.85	19.6	0.4	VU DUR
TAN 20-C	8885312	669333	1.649E-09	0.561	0.004	0.368	0.7	0.0	20.9	0.81	25.7	0.5	VU DUR
TAN 20-D	8885312	669333	5.869E-10	0.295	0.002	0.234	0.8	0.0	13.8	0.77	18.0	0.4	VU DUR
TAN 16-1	8885628	669212	1.041E-09	0.377	0.003	0.076	0.2	0.0	21.7	0.71	30.4	0.8	CT DUR
TAN 16-2	8885628	669212	8.401E-10	0.308	0.002	0.066	0.2	0.0	21.4	0.73	29.2	0.7	CT DUR
TAN 17-A	8892500	664893	2.102E-10	0.081	0.001	0.247	3.1	0.1	12.4	0.77	16.2	0.3	VU DUR
TAN 17-C	8892500	664893	2.896E-11	0.016	0.000	0.067	4.3	0.1	7.6	0.88	8.7	0.3	VU DUR
TAN 18-A	8890311	666454	2.653E-10	0.140	0.001	0.478	3.4	0.1	8.6	0.86	10.0	0.2	VU DUR
TAN 18-B	8890311	666454	8.346E-11	0.068	0.000	0.172	2.5	0.0	6.3	0.83	7.6	0.1	VU DUR
TAN 18-C	8890311	666454	1.157E-10	0.098	0.001	0.419	4.3	0.1	4.8	0.82	5.8	0.1	VU DUR
Standards													
CT DUR			9.567E-09	0.431	0.003	8.492	19.7	0.3	32.4				
CT DUR			5.844E-09	0.270	0.002	5.745	21.3	0.3	29.6				
VUDUR48			4.561E-09	0.172	0.001	3.998	23.3	0.4	33.6				
VUDUR49			3.048E-09	0.123	0.001	2.569	20.8	0.3	34.3				

Table 1: Analytical data for AHe samples along the rift shoulder of the North Basin, Malawi Rift. CT DUR and VU DUR are Durango standards obtained from Ken Farley at Caltec and from Tibor Dunai, Vrije Universiteit respectively. Amp Gneiss = amphibolites gneiss.
Note for Tan 07: He contribution from the blank is significant (15%), however there is sufficient U and Th to include this age in the analyses. The low He contained in the sample is probably due to its young age.

Table 2

Click here to download Table: mortimer et al table 2.docx

Table 2: Apatite He age and elevation data for samples from the North Basin, Malawi Rift.

Sample	Age (Ma) †	± 2σ(Ma)	Elevation (m)
Livingstone summit and plateau			
TAN10	197.4	2.7	2194
TAN14	163.7	9.9	1569
Livingstone Fault escarpment (North segment)			
TAN3	14.2*	1.1	550
TAN7	2.1	1.3	489
TAN9	12.1	3.5	450
Livingstone Fault escarpment (Central and South segments)			
TAN15	22.5	3.4	1270
TAN20	21.6	9.2	673
TAN16	29.7	1.2	548
TAN17	12.5	7.5	538
TAN18	7.1	3.2	509

† All ages calculated from weighted average of replicates following correction except those indicated by * where ages were not replicated. The location of samples is shown in Figure 1.

Supplementary material for online publication only

Click here to download Supplementary material for online publication only: appendix a.jpg